Exact Calculation of the Penetrability Through Two-Peaked Fission Barriers*

J. D. Cramer and J. R. Nix
University of California, Los Alamos Scientific Laboratory, Los Alamos, New Mexico 87544
(Received 2 March 1970)

The penetrability is computed exactly for a fission barrier $V(\epsilon)$ defined in terms of two parabolic peaks connected smoothly with a third parabola forming the intermediate well. The potential is specified by the peak energies E_1 and E_3 and the minimum energy E_2 of the connecting curve, along with the constants $\hbar\omega_1$, $\hbar\omega_3$, and $\hbar\omega_2$ related to the curvatures of the three parabolas. For an incident wave of unit amplitude, the amplitude of the transmitted wave is determined by requiring that the wave functions (expressed exactly in terms of parabolic-cylinder functions) and their first derivatives match at the points where the parabolas are connected. The penetrability is then obtained from the amplitude of the transmitted wave. The transmission is essentially an increasing exponential function exhibiting narrow resonances at the positions of quasibound states in the intermediate well. The widths of these resonances are extremely small (~10 eV) for the levels near the bottom of the well but increase dramatically as the energy increases. This trend continues in some cases above the top of the barrier, producing broad peaks in the penetrability function. The exact penetrabilities are accurately reproduced by the WKB approximation for energies well below the barrier tops, but for energies near the barrier tops the WKB approximation is found to overestimate the penetrability for the cases studied.

I. INTRODUCTION

A semiempirical method for describing the influence of single-particle shell effects on nuclear ground-state masses and deformations was introduced a few years ago by Myers and Swiatecki.[1] Soon after this development, Strutinsky proposed a systematic technique for determining the magnitude of these shell effects as they varied with nuclear deformation.[2] When this method was applied to the large deformations appropriate to fission in actinide nuclei, peaks and depressions became apparent in the potential energy of deformation. From these theoretical results, a more complicated picture of the fission barrier began to emerge. An idealization of this potential barrier is two peaks separated by an intermediate well.

Several recently observed fission phenomena have been interpreted in the light of these theoretical predictions of an intermediate well in the nuclear potential energy of deformation. The lowest-lying state in this intermediate well was theorized[2] to be the source of the spontaneously fissioning isomer of ^{242}Am first observed by Polikanov *et al.*[3] Still additional experimental evidence began to appear. Clusters of subthreshold fission were observed in the neutron-induced fission of ^{240}Pu and ^{237}Np target nuclei.[4-6] It was observed that the resonance grouping of these subthreshold levels could be explained by a modulation of fission strength through broad resonances near the top of the intermediate well.[5,7]

Anomalies have long been apparent in fission cross-section data. For example, the sharp structure observed in the ^{234}U(n,f), ^{230}Th(n,f), and ^{239}Pu(d,pf) reaction data[8-11] near the fission threshold had never been adequately explained. The presence of broad levels near the top of this intermediate well can qualitatively explain this anomalous structure.

Investigators involved in systematic searches for the short-lived spontaneously fissioning isomers have recently disclosed the existence of these isomers in many of the accessible actinide nuclei.[12-15]

Further theoretical studies of shell effects on the fission barrier[16,17] have corroborated the early work, and strongly indicate the presence of at least one – and possibly two – intermediate wells in the nuclear potential energy of deformation. Extensive discussions of the consequences of the two-peaked character of the fission barrier have been provided by Lynn[9] and by Bjørnholm and Strutinsky.[18]

Central to the description of the consequences of a two-peaked fission barrier is the quantitative problem of calculating the probability that the nucleus will penetrate a barrier of this shape. The well-known Hill-Wheeler formulation[19] for the penetration of a single parabolic barrier no longer serves as an adequate description of the fission process. Several alternative penetrability calculations have recently been presented. A numerical-integration method[20] was used in a model to describe structure observed in fission probabilities obtained in recent (d,pf) experiments.[21] A technique utilizing the WKB (quasiclassical) approximation has been proposed as an alternative method for computing the penetrabilities of two-peaked barriers having a completely general shape.[22,23]

Concurrent efforts have provided an exact meth-

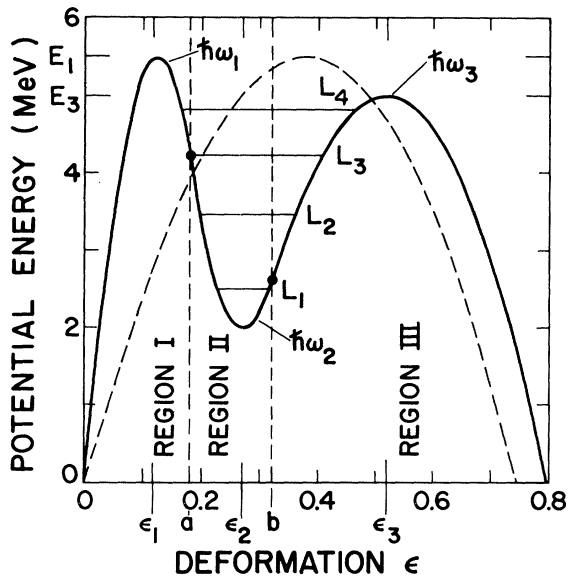

FIG. 1. An illustration of a two-peaked fission barrier parametrized by portions of three smoothly joined parabolas. The connecting points a and b define three regions of the potential energy. The locations L_i of the quasibound levels are indicated. The dashed curve represents a comparable single parabolic barrier. Parameters for this barrier are listed in Table I.

od of calculating the penetrability function for barriers that are constructed of three connecting parabolas to define two peaks with an intermediate well.[24,25] Such an exact calculation has been incorporated into a fission model that was used to describe direct-reaction fission data.[26,27] However, these previously published works have included only brief mention of the computational technique; we intend here to describe the calculation in sufficient detail so that it can be used by others.

A second purpose of this paper is to explore the influence of variations of the shape of the potential barrier on the penetrability, and to relate the consequences of these variations to general observations in experimental data. In addition, the exact calculations are compared with results of the WKB (quasiclassical) approximation[22,23] for both symmetric and asymmetric barrier shapes. A brief discussion of the penetrabilities of rectangular two-peaked barriers is also included.

II. PENETRABILITY CALCULATION

Consider a one-dimensional potential barrier constructed of three connected parabolas. If one assumes that the inertial parameter is constant in each of the three regions separated by the connecting points of the parabolas, an exact solution of the Schrödinger equation of the system is possible. The energy-dependent probability that a penetration will occur for a single assault on this potential barrier – the penetrability function – can then be determined from the solutions of the Schrödinger equation.

A typical potential barrier to be considered for this computation is shown by the solid line in Fig. 1. The equation for this potential is

$$V(\epsilon) = E_i \pm \tfrac{1}{2}\mu\omega_i^2(\epsilon - \epsilon_i)^2, \quad i = 1,\ 2,\ 3, \tag{1}$$

where ϵ denotes the nuclear-deformation coordinate in the fission degree of freedom. The three regions $i = 1,\ 2,\ 3$ are separated by the connecting points a and b of the three parabolic curves shown in Fig. 1. The minus sign in Eq. (1) refers to the two peak regions (regions I and III in the figure), and the plus sign refers to the region of the intermediate well (region II). The energies E_i are the maximum or minimum values of the potential at the deformations ϵ_i; the "frequencies" ω_i determine the widths of the individual portions of the barrier. The inertial parameter μ represents the effective mass of the system with respect to distortions in the ϵ direction.

We have chosen to connect the three parabolas smoothly by requiring the first derivatives of $V(\epsilon)$ to be continuous at the two connecting points a and b. This reduces the number of parameters required to completely specify the potential energy of deformation from nine to seven. In addition, the potential is translationally invariant, and this can be used to further reduce the number of parameters to six. These six parameters are chosen to be the three energies E_i and the three frequencies ω_i. The values ϵ_i of the deformation corresponding to the three extrema in the potential, as well as the two connecting points a and b, are then determined in terms of these six basic parameters. This is discussed in more detail in the Appendix.

The Schrödinger equation for this system can be written as

$$\frac{d^2}{d\epsilon^2}\Psi(\epsilon) + \frac{2\mu}{\hbar^2}[E - V(\epsilon)]\Psi(\epsilon) = 0\,. \tag{2}$$

The solutions of this equation are expressed as linear combinations of parabolic-cylinder functions, selected to clearly identify and separate transmitted waves from reflected waves. There exists a right-left degeneracy in this system, and the solutions to Eq. (2) are chosen to allow the initial wave of amplitude A to impinge on the barrier from left to right. The solutions for the three regions are then

$$\Psi(\epsilon) = \begin{cases} A\psi_1(\rightarrow) + B\phi_1(\leftarrow), & \epsilon \leq a \\ C\delta_2 + D\eta_2, & a \leq \epsilon \leq b \\ T\psi_3(\rightarrow), & b \leq \epsilon, \end{cases}$$

where the direction of the phase velocity is indicat-

ed by the arrows in parentheses. We are considering only those cases for which the reflection amplitude in region III is zero. It is not important to identify the direction of the phase velocity for the wave functions δ_2 and η_2 in the intermediate region (region II), since their amplitudes do not enter the penetrability problem explicitly. The requirement that these wave functions and their derivatives be continuous at the connecting points a and b yields four linear equations containing five unknown amplitudes. These equations are then solved for the ratio of the transmitted amplitude T to the incident amplitude A and substituted into the relationship which determines the penetrability,

$$P = (\omega_3/\omega_1)^{1/2} \, |T/A|^2 .$$

The curvature parameters ω_1 and ω_3 appear in the formula because of the conservation of probability currents. The energy dependence of the penetrability is obtained by evaluating T/A for different values of incident energy. Barrier parameters that were used in this sample calculation are listed in Table I. A more detailed development of these results is outlined in the Appendix.

If the effective mass μ in Eqs. (1) and (2) is assumed to be constant over the entire region, the penetrability function is independent of μ, and its only purpose is to scale the potential energy of deformation. The value used for μ was obtained from the semiempirical result[16,28]

$$\mu = 0.0540 A^{5/3} \hbar^2/\mathrm{MeV},$$

where A is the nuclear mass number.

III. RESULTS OF CALCULATION

The penetrability function for the two-peaked potential barrier of Fig. 1 is given by the solid curve in Fig. 2. The energy and maximum penetrability of the subthreshold fission resonances are indicated by the vertical lines. The enhanced penetration at these points is a direct result of the existence of the quasibound states L_1 through L_4 in the intermediate well of the potential shown in Fig. 1. The resonances due to the low-lying levels are typically very narrow (see the column labeled FWHM in Table II). For the levels near the top of the well the resonances are broader. The resonance parameters for this example are listed in Table II; the peak values of the penetrabilities are given in the column labeled $P_{\max}$. These resonance parameters were determined by a procedure that selects the Lorenzian curve that best fits the calculated penetrabilities at every resonance.

TABLE I. Parameters for the fission barriers of Fig. 1.

	Two-peaked barrier	Single parabolic barrier
Nuclear mass number A	240	240
E_1	5.50 MeV	5.50 MeV
$\hbar\omega_1$	1.25 MeV	0.40 MeV
E_2	2.00 MeV	
$\hbar\omega_2$	1.00 MeV	
E_3	5.00 MeV	
$\hbar\omega_3$	0.50 MeV	
Spontaneous-fission half-life	2.45×10^{12} yr	3.3×10^{9} yr
Isomeric half-life	48 nsec	none

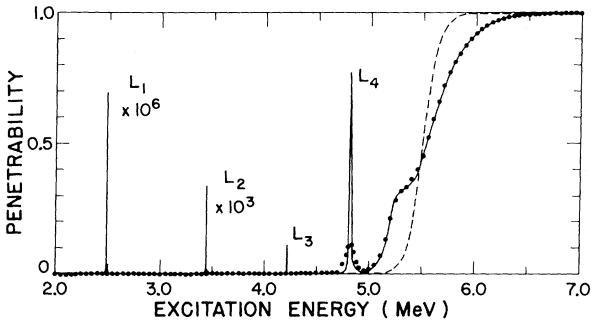

FIG. 2. A linear plot of the calculated penetrability through the two-peaked barrier of Fig. 1. Note the sharp resonances at the positions of the quasibound levels in the intermediate well. To illustrate the influence of experimental resolution, the solid points represent the results of folding the calculated penetrability with a Gaussian function having a full width at half maximum of 100 keV. The dashed curve gives the penetrability for the single parabolic barrier of Fig. 1.

To demonstrate the effect that experimental resolution broadening might have on these peaks in the penetrability functions, the calculated penetrability was broadened with a normalized Gaussian function of 100 keV full width at half maximum (FWHM). These experimentally broadened results are indicated by the points in Fig. 2.

As the incident energy E approaches the peak energies of the potential barrier (approximately 5 MeV in this case), the penetrability becomes a smoothly increasing function to its maximum value of unity. There is mild structure, however, in

TABLE II. Subthreshold fission resonances for the two-peaked barrier of Table I.

Level	Energy (MeV)	FWHM (keV)	$P_{\max}$
L_1	2.492	$\approx$0.01	0.699×10^{-6}
L_2	3.430	$\approx$0.10	0.349×10^{-3}
L_3	4.215	0.196	0.115
L_4	4.811	9.464	0.785

this energy region, as illustrated by the "step" beginning at 5.25 MeV. This feature corresponds to a very broad unbound level which lies below the higher peak but above the lower peak in the potential energy of deformation. A structure similar to this is observed in the (n,f) cross section for several nuclei.

The dashed curve in Fig. 2 shows the familiar results corresponding to penetrating a single parabolic barrier, as discussed by Hill and Wheeler,[19]

$$P(E) = \{1 + \exp[2\pi(E_0 - E)/(\hbar\omega_0)]\}^{-1}.$$

Here $P(E)$ is the energy-dependent penetrability, E_0 is the peak height of the barrier, E is the incident energy, and $\hbar\omega_0$ is the curvature parameter of the barrier. This single parabolic barrier is shown in Fig. 1 by the dashed curve. Values of the barrier parameters used in this calculation are also listed in Table I. Although this barrier is comparable to the two-peaked barrier, in the sense of having the same height and predicting approximately the same spontaneous-fission lifetime, there are notable differences in their penetrability functions. In addition to the obvious absence of any resonance penetration, the single-barrier penetrability rises much more rapidly than the penetrability for the two-peaked barrier.

To state it in another way, a single fission barrier allows a much more rapid opening of the fission channels or transition states than does a comparable two-peaked barrier. The influence of this effect is observed in experimental fission probabilities at excitation energies near the top of the barrier.[11,27] For all of the nuclei studied in the experimental work cited, the slopes of the fission probabilities are considerably smaller than the slopes predicted by penetration through a realistic single barrier.

Additional information can be obtained from this parametrization of the fission barrier which correlates with existing experimental information. The known spontaneous-fission lifetimes of the various nuclei can be used to provide a measure of the barrier area. These half-lives can be calculated with the barrier model and compared to measured values as outlined in the Appendix. The half-lives determined for the sample barriers of Fig. 1 are listed in Table I. The value of 2.45×10^{12} yr for the two-peaked barrier is in general agreement with the spontaneous-fission half-lives for Pu and U isotopes.

As mentioned earlier, the short-lived spontaneously fissioning isomers can be understood on the basis of a two-peaked potential. These shape isomers are situated at a deformation corresponding to the intermediate well. The half-life of this isomeric state can be computed from the parameters of the potential barrier described in this study. Details of these computations are outlined in the Appendix. The calculated isomeric half-life for the sample barrier in Fig. 1 is 48 nsec, as listed in Table I. Recent experiments involving the search for such isomers have discovered isomeric half-lives ranging from 10^{-2} to 10^{-9} sec. It was indicated earlier that the penetrability calculations are insensitive to a right-left orientation of asymmetric barriers; i.e., mirror-image barriers have the same penetrability. There is, however, a selective mechanism inherent in the isomer decay that could eliminate this right-left degeneracy. The isomeric lifetime must be determined from both modes of decay from the intermediate well: γ decay to the left and spontaneous fission to the right. It has been pointed out,[29] however, that the γ decay from the shape-isomeric state is inhibited relative to spontaneous fission by a factor of approximately 10^7 because of the competition between γ decay to a final ground state and a return to the intermediate well. Decay from a symmetric barrier is therefore almost exclusively spontaneous fission. On the other hand, the asymmetric barrier would have a much shorter isomeric lifetime if the thinner peak were on the right – toward the scission direction – rather than on the left, as in the sample barrier of Fig. 1.

IV. EFFECTS OF PARAMETER VARIATIONS

As suggested earlier, the general size of the fission barrier can be determined experimentally by fission cross-section measurements and fission probability measurements (which determine the approximate height of the barrier) and spontaneous-fission lifetime measurements (which determine the total area of the barrier). It further appears that right-left degeneracies can be resolved for the asymmetric barriers by measured lifetimes of the shape isomers. These factors constitute the constraints which must be met in defining a realistic potential energy barrier for the fission of heavy nuclei.

It remains then to explore the effects that varying the barrier shape has on the penetrability function, within the bounds of the above general criteria.

In contrast to the asymmetric barrier of Fig. 1, the symmetric barrier yields uniform peak heights closely approximating unity in the computed penetrability at the resonance energies. An example of a symmetric barrier and the resulting penetrability is shown in Fig. 3. The potential energy of deformation is shown on the left and the logarithm of the penetrability, calculated by the exact method, is indicated by the solid line on the right. The pa-

rameters that describe this barrier are listed in Table III. The positions of the resonances occur very near the incident energies

$$E_n = E_2 + (n + \tfrac{1}{2})\hbar\omega_2 ,$$

which are the energy levels that would occur if the intermediate harmonic-oscillator potential well were extended to infinity. Since the perturbation required to transform an intermediate parabolic well into a two-peaked barrier is negative, the actual resonances occur at somewhat lower energies. The maximum downward shift from the above harmonic-oscillator spacing is approximately 0.1% and occurs for the highest resonance.

This leads us into a discussion of the effects of varying the curvature parameter $\hbar\omega_2$ and the depth E_2 of the intermediate well. Because of the approximate validity of the above harmonic-oscillator spacing rule, the distance between resonances decreases as the intermediate well becomes wider (corresponding to smaller values of $\hbar\omega_2$), and vice versa. The depth of the well E_2 has a double influence. First, the number of levels increases as the well becomes deeper when $\hbar\omega_2$ is held fixed. Second, the isomeric lifetime increases as the well becomes deeper.

TABLE III. Parameters for the symmetric and asymmetric two-peaked fission barriers of Figs. 3 and 4.

	Symmetric	Asymmetric
Nuclear mass number A	240	240
E_1	6.0 MeV	6.0 MeV
$\hbar\omega_1$	1.0 MeV	1.3 MeV
E_2	2.0 MeV	2.0 MeV
$\hbar\omega_2$	0.5 MeV	2.0 MeV
E_3	6.0 MeV	5.0 MeV
$\hbar\omega_3$	1.0 MeV	0.48 MeV
Spontaneous-fission half-life	1.95×10^{17} yr	4.61×10^{11} yr
Isomeric half-life	18.4 nsec	0.33 nsec

To illustrate the influence of the peak heights E_1 and E_3 on the penetrability function, we will first consider the significance of the average of these two values. And, for comparison with single-barrier penetration, it is necessary to select the incident energy $E_{1/2}$ at which the penetrability is equal to 0.5. This value corresponds to the peak energy for single parabolic barriers. For the asymmetric barrier described in Fig. 1 and Table I, the value

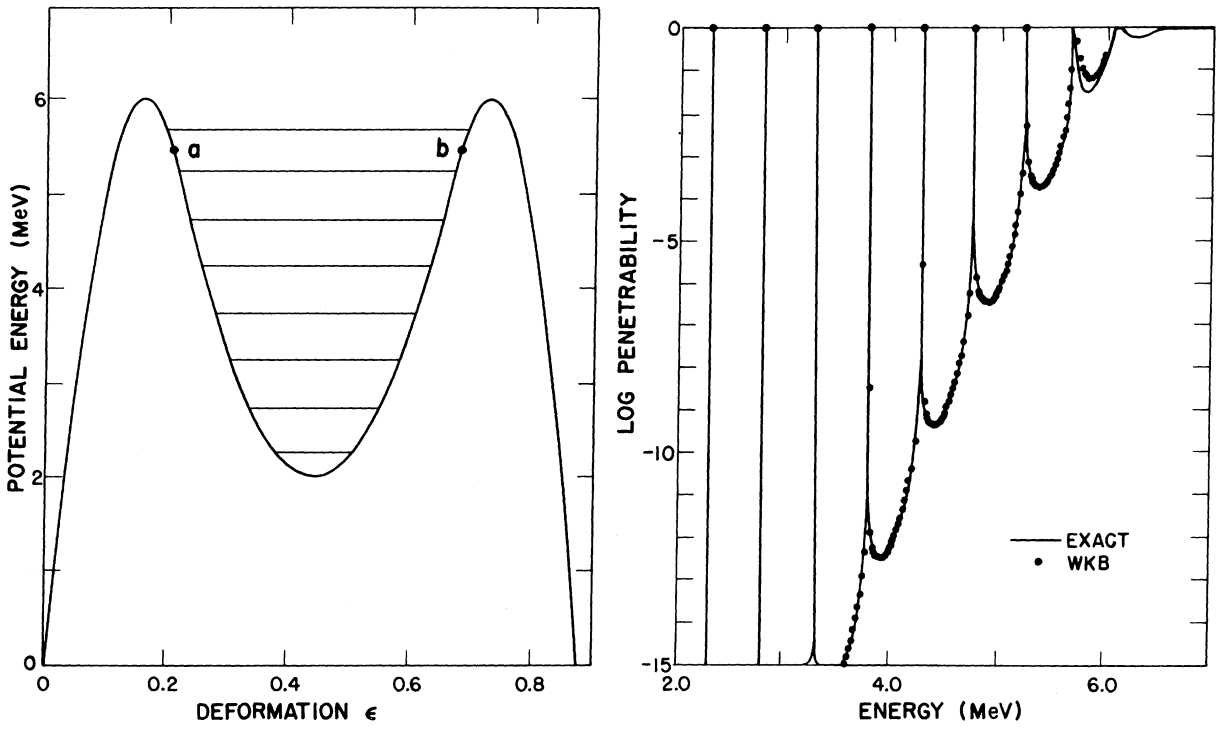

FIG. 3. A comparison of exact and WKB (quasiclassical) penetrabilities for a symmetric barrier. The potential barrier is shown on the left, with the connecting points a and b and the positions of the quasibound levels indicated. The semi-log plot on the right compares the exact results (solid line) and the WKB results (solid points). The energy shift indicated here at the 5.70-MeV resonance between the WKB and exact methods is 30 keV. The predicted penetrabilities in the valley just above the 5.70-MeV resonance are 6.1×10^{-2} and 3.1×10^{-2} for the WKB and exact methods, respectively. Parameters for this barrier are listed in Table III.

of $E_{1/2}$ is 5.55 MeV and the average peak height is 5.25 MeV. The value of $E_{1/2}$ for the symmetric barrier described in Fig. 3 and Table III is 6.06 MeV, and the average peak height is 6.0 MeV. In general, the half-value penetrability occurs at energies above the average energy of the two peaks and, on occasion, even slightly above the higher peak energy.

In the case of asymmetric barriers, the slope of the penetrability function near its maximum is determined by the curvature of the higher peak in the potential. Therefore, the relative height of the broad and narrow peaks can be determined from the shape of the penetrability function. If the narrower peak corresponding to a larger value of $\hbar\omega$ is higher, the slope is more gentle, and vice versa.

This brief discussion has been an attempt to summarize the effects on the penetrability of varying individual parameters. However, the situation is more complicated when several parameters are varied simultaneously, and no attempt will be made here to enumerate such effects.

V. COMPARISON OF THE EXACT CALCULATION TO OTHER RESULTS

A WKB (quasiclassical) approximation has recently been developed[22,23] for determining penetrabilities through two-peaked barriers. In the notation of Ref. 23, the penetrability in the WKB approximation was determined to be

$$P(E) = 64P_A P_B[(P_A P_B + 16)^2\cos^2\varphi + 16(P_A + P_B)^2\sin^2\varphi]^{-1}, \quad (3)$$

where P_A and P_B are the penetrabilities through the two individual peaks A and B, respectively, at incident energy E. The energy-dependent phase φ is given by the integral

$$\varphi(E) = \int_\alpha^\beta \left(\frac{2\mu}{\hbar^2}[E - V(\epsilon)]\right)^{1/2} d\epsilon. \quad (4)$$

The limits of integration α and β are the values of ϵ on the inner sides of the two peaks at which the integrand vanishes.

This description of the WKB penetrability is valid over a limited range of incident energies. Although this method could be generalized,[30] the lower limit of applicability of this formulation is the bottom of the intermediate well, and the upper limit is the top of the lowest peak. This, unfortunately, does not cover the region of incident energy where most of the fission cross-section data and fission probability information are available. Ow-

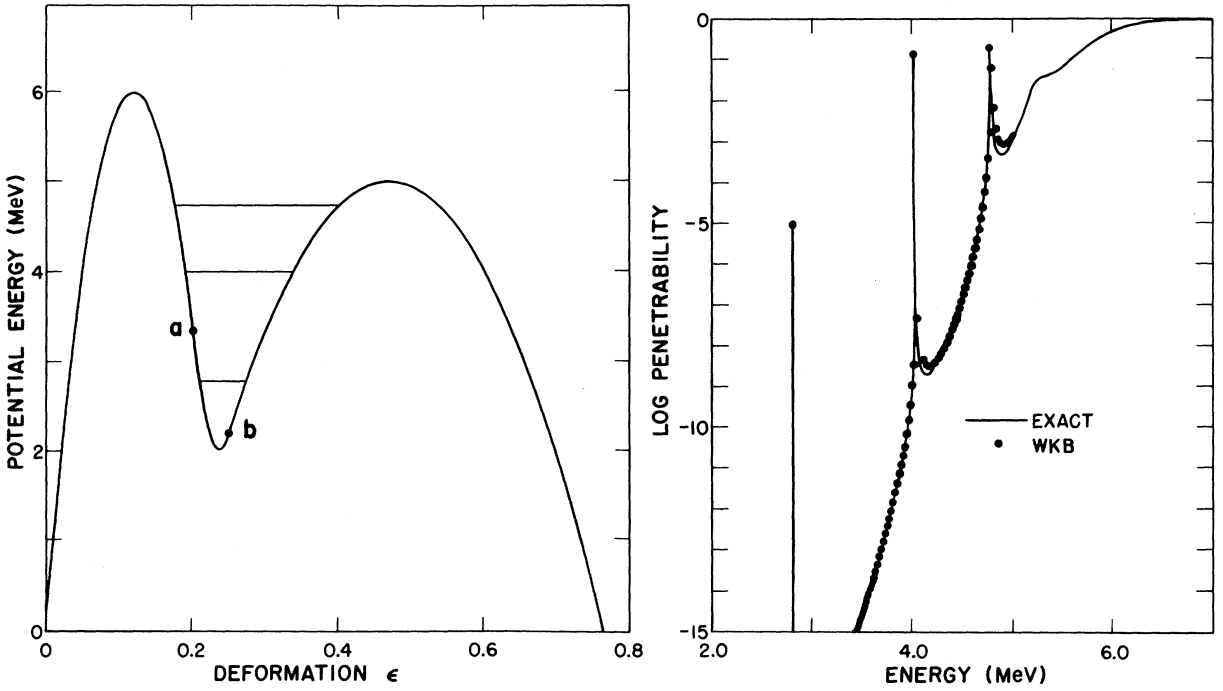

FIG. 4. A comparison of exact and WKB (quasiclassical) penetrabilities for an asymmetric barrier. The potential barrier is shown on the left, with the connecting points a and b and the positions of the quasibound levels indicated. The semilog plot on the right compares the exact results (solid line) and the WKB results (solid points). The energy shift indicated here at the 4.76-MeV resonance between the WKB and exact methods is 20 keV. The predicted penetrabilities in the valley just above the 4.76-MeV resonance are 8.4×10^{-4} and 5.2×10^{-4} for the WKB and exact methods, respectively. Parameters for this barrier are listed in Table III.

ing primarily to the experimental need for reasonable counting rates, most of these data are nonexistent at energies of more than 200–300 keV below the highest peak in the fission barrier.

We have used the WKB method to calculate the penetrability through a fission barrier described by three smoothly connected parabolas and have compared the results with the exact penetrabilities. Examples of such comparisons are shown in Figs. 3 and 4 for symmetric and asymmetric barriers, respectively. The parameters used to describe these barriers are listed in Table III. The results of the exact calculation are shown by the solid lines, and those of the WKB approximation by the solid points.

Considering first the symmetric case of Fig. 3, it is apparent that in general both methods agree very well. However, there are two basic differences apparent in the comparison, and both occur near the top of the well. First, the WKB method predicts level positions at the points where the phase is given by

$$\varphi = (n+\tfrac{1}{2})\pi, \quad n = 0,\ 1,\ 2, \ldots .$$

This prediction is correct for an infinite parabolic well, where there is no possibility of leakage through the sides. When the well if finite, as in the case in question, these levels are depressed by an amount which can be determined from first-order perturbation theory. The magnitude of this effect is small, but visible in Fig. 3. The second difference is more apparent in the figure. The WKB penetrability is greater in the valleys just above the resonances in the upper part of the well. This is the region where this formulation of the WKB method is reaching its upper limit of applicability.

With few exceptions, the comparison for the asymmetric case of Fig. 4 displays the same characteristics as have been discussed for the symmetric case. Notably different in the asymmetric case are the peak heights and the lower upper limit of the WKB formulation. It can be seen from Eq. (3) that in the WKB formulation the maximum penetrability at the peaks is given by

$$P_{\max} = 4P_A P_B/(P_A + P_B)^2 .$$

As indicated in Fig. 4, these peak values agree with those predicted by the exact calculation.

In the course of this study, the penetration of rectangular-shaped barriers was also briefly considered. Appropriate barriers were constructed to predict isomeric and spontaneous-fission lifetimes which were comparable to predictions of the smooth barriers of Figs. 3 and 4. An exact calculation of the penetrability of these barriers was carried out as before, by matching wave functions and their derivatives. At incident energies below the peak heights, the penetrabilities were generally not unlike those computed for the smooth barriers. For instance, the symmetric rectangular barrier predicts resonances that are spaced at increasing intervals, which correspond to the levels predicted by Eq. (4) of the WKB method. The primary difference observed in a comparison of rectangular barriers to smooth barriers is the oscillatory character of the penetrability through rectangular barriers at incident energies above the peaks. This is due primarily to the effect of the sharp corners on the potential curve. In analogy, this effect is similar to light transmission in thin refracting layers. When the product of the wave number and the individual barrier thickness is equal to odd multiples of $\pi/2$, interference characteristics inhibit transmission.

VI. SUMMARY AND CONCLUSION

Both theory and experiment have recently suggested that the fission barriers of actinide nuclei are two peaked. We have considered here the calculation of the penetrability through two-peaked barriers, defined in terms of smoothly joined portions of three parabolas. This parametrization of the barrier was made for two reasons: First, the penetrability through such a barrier can be computed exactly in terms of known functions. Second, such a barrier is described by a total of six parameters – three heights and three widths – which are the number and type of quantities that can be related to experimental data.

The penetrabilities computed for this six-parameter potential by this relatively simple method allows one to explore the influences of a wide variety of fission barrier shapes as they apply to experimental information. A few examples of individual-parameter variations and their relation to experimental data were discussed in Sec. IV.

The exact penetrabilities were compared in Sec. V with results of a WKB (quasiclassical) approximation for both symmetric and asymmetric barriers. Although both methods produce similar results at energies well below the peaks, increasing differences appear in the penetrabilities as the incident energy approaches the top of the barriers.

Future analyses of experimental fission data will require a consideration of the two-peaked nature of the barrier. It is hoped that our calculations of the penetrability through two-peaked barriers will prove useful for this purpose.

ACKNOWLEDGMENT

We would like to thank Harold C. Britt for his many useful suggestions regarding this study.

APPENDIX. DETAILS OF THE CALCULATION

The probability that a potential barrier $V(\epsilon)$ is penetrated at a given incident energy E is determined from the probability current for the system under consideration, which in turn is obtained by solving the Schrödinger equation.

A. Potential Energy

Consider first the nuclear potential energy V of the system as a function of the deformation ϵ, as illustrated in Fig. 1,

$$\begin{aligned} V(\epsilon) &= E_1 - \tfrac{1}{2}\mu\omega_1^2(\epsilon-\epsilon_1)^2, \quad \epsilon \le a, \\ &= E_2 + \tfrac{1}{2}\mu\omega_2^2(\epsilon-\epsilon_2)^2, \quad a \le \epsilon \le b, \\ &= E_3 - \tfrac{1}{2}\mu\omega_3^2(\epsilon-\epsilon_3)^2, \quad b \le \epsilon. \end{aligned} \tag{5}$$

The energies E_1 and E_3 are the maximum values of the potential at the deformations ϵ_1 and ϵ_3, respectively, and E_2 is the minimum value at ϵ_2. The curvatures at these points are $\mu\omega_1^2$, $\mu\omega_3^2$, and $\mu\omega_2^2$, respectively, where μ is the effective mass for motion in the ϵ direction; it is assumed to be constant for all values of ϵ.

The barrier defined by Eq. (5) is seen to contain a total of nine parameters, three to describe each of the three parabolas. Two of the nine parameters are eliminated, however, by the requirement that the outer parabolas join smoothly at the intersection points a and b, rather than with discontinuous first derivatives. Another parameter is eliminated if one allows an arbitrary choice of the absolute location of the barrier on the ϵ axis. This reduces the number of parameters required to specify the barrier to six. These are chosen to be the three energies E_1, E_2, and E_3 and the three frequencies ω_1, ω_2, and ω_3. By arbitrarily setting

$$V(\epsilon) = 0 \quad \text{at } \epsilon = 0,$$

the remaining quantities can be expressed in terms of the six basic parameters as follows:

$$\begin{aligned} \epsilon_1 &= (2E_1/\mu\omega_1^2)^{1/2}, \\ a &= \epsilon_1 + [2(E_1-E_2)/\mu\omega_1^2]^{1/2}(1+\omega_1^2/\omega_2^2)^{-1/2}, \\ \epsilon_2 &= a + [2(E_1-E_2)/\mu\omega_2^2]^{1/2}(1+\omega_2^2/\omega_1^2)^{-1/2}, \\ b &= \epsilon_2 + [2(E_3-E_2)/\mu\omega_2^2]^{1/2}(1+\omega_2^2/\omega_3^2)^{-1/2}, \\ \epsilon_3 &= b + [2(E_3-E_2)/\mu\omega_3^2]^{1/2}(1+\omega_3^2/\omega_2^2)^{-1/2}. \end{aligned}$$

B. Wave Functions

The Schrödinger equations for this potential are written as

$$\frac{d^2}{d\epsilon^2}\Psi_i + \frac{2\mu}{\hbar^2}[E - E_i \pm \tfrac{1}{2}\mu\omega_i^2(\epsilon-\epsilon_i)^2]\Psi_i = 0, \tag{6}$$

where the plus sign applies when i refers to region I or III in Fig. 1 and the minus sign applies when i refers to region II. There is a right-left degeneracy inherently associated with a one-dimensional Schrödinger equation. The case for initial momentum transfer from left to right has been arbitrarily selected, yielding solutions to Eqs. (6) of the form

$$\begin{aligned} \Psi_{\mathrm{I}} &= A\psi_1(\rightarrow) + B\varphi_1(\leftarrow), \quad \epsilon \le a, \\ \Psi_{\mathrm{II}} &= C\delta_2 + D\eta_2, \quad a \le \epsilon \le b, \\ \Psi_{\mathrm{III}} &= T\psi_3(\rightarrow), \quad b \le \epsilon, \end{aligned} \tag{7}$$

where the functions $\psi_i(\rightarrow)$ represent wave packets with phase velocity moving to the right, and the function $\varphi_1(\leftarrow)$ represents a reflected component traveling to the left. The functions δ_2 and η_2 in the region of the intermediate well can each be mixtures of waves traveling in both directions, since the final result does not contain the amplitudes C and D explicitly.

The Schrödinger equations (6) represent a general class of second-order differential equations which in standard form are

$$d^2y/du^2 + (\tfrac{1}{4}u^2 - \alpha)y = 0 \tag{8a}$$

and

$$d^2y/dv^2 - (\tfrac{1}{4}v^2 + \alpha)y = 0. \tag{8b}$$

The solutions to these equations are Weber's parabolic-cylinder functions.[31] To reduce the Schrödinger equations (6) to this form, we make the substitutions

$$\begin{aligned} u &= (2\mu\omega_1/\hbar)^{1/2}(\epsilon-\epsilon_1), \quad \alpha_1 = (E_1-E)/\hbar\omega_1, \\ v &= (2\mu\omega_2/\hbar)^{1/2}(\epsilon-\epsilon_2), \quad \alpha_2 = (E_2-E)/\hbar\omega_2, \\ w &= (2\mu\omega_3/\hbar)^{1/2}(\epsilon-\epsilon_3), \quad \alpha_3 = (E_3-E)/\hbar\omega_3. \end{aligned}$$

It is essential to select the proper linear combinations of parabolic-cylinder functions for the wave functions $\psi_i(\rightarrow)$ and $\varphi_1(\leftarrow)$ of Eqs. (7) in regions I and III to clearly identify the directions of phase velocity. The asymptotic behavior of the functions at large values of positive and negative ϵ indicates the proper combination of functions.

The wave functions for regions I and III become

$$\begin{aligned} \psi_1(\rightarrow) &= E^*(\alpha_1, -u), \\ \varphi_1(\leftarrow) &= E(\alpha_1, -u), \\ \psi_3(\rightarrow) &= E(\alpha_3, w), \end{aligned} \tag{9}$$

where the function $E(\alpha, x)$ is the complex linear combination

$$E(\alpha, x) = k^{-1/2}W(\alpha, x) + ik^{1/2}W(\alpha, -x)$$

of the fundamental parabolic-cylinder function $W(\alpha, x)$[31]; the quantity k is defined by

$$k = (1 + e^{2\pi\alpha})^{1/2} - e^{\pi\alpha}.$$

In region II, the solutions to the Schrödinger equation can be written in the form of the standard parabolic-cylinder solutions U and V[31] for the differential equations (8), namely,

$$\delta_2 = U(\alpha_2, v) \quad \text{and} \quad \eta_2 = V(\alpha_2, v). \tag{10}$$

The wave functions are conveniently evaluated in practice by use of their known series expansions.[31]

C. Penetrability

If the probability current is conserved, it follows that the penetrability is given by

$$P = (\omega_3/\omega_1)^{1/2} \, |T/A|^2 . \tag{11}$$

The wave-amplitude ratio T/A is determined by requiring that the wave functions [given by Eqs. (7)] and their derivatives with respect to the deformation coordinate ϵ be continuous at the connecting points a and b. These conditions are expressed in terms of four linear equations which can be solved by Cramer's rule for the desired amplitude ratio. The result is conveniently expressed as the product of two Wronskians divided by the determinant of a 4×4 matrix,

$$\frac{T}{A} = \frac{v'u'W[E^*(\alpha_1, -u), E(\alpha_1, -u)]W[U(\alpha_2, v), V(\alpha_2, v)]}{\begin{vmatrix} E_a(\alpha_1, -u) & -V_a(\alpha_2, v) & -U_a(\alpha_2, v) & 0 \\ -u'E_a^{(-u)}(\alpha_1, -u) & -v'V_a^{(v)}(\alpha_2, v) & -v'U_a^{(v)}(\alpha_2, v) & 0 \\ 0 & V_b(\alpha_2, v) & U_b(\alpha_2, v) & -E_b(\alpha_3, w) \\ 0 & v'V_b^{(v)}(\alpha_2, v) & v'U_b^{(v)}(\alpha_2, v) & -w'E_b^{(w)}(\alpha_3, w) \end{vmatrix}} . \tag{12}$$

The primes on the variables u, v, and w indicate differentiation with respect to the deformation parameter ϵ and are simply constants, the symbol W denotes the Wronskians of the indicated functions, and the subscripts a and b on the parabolic-cylinder functions indicate the points where the functions are to be evaluated. First-order differentiation with respect to the argument u, v, or w is indicated by a superscript inside parentheses. The values of the two Wronskians appearing in the numerator are constants and are equal to $2i$ and $\sqrt{2/\pi}$, respectively.

It is of interest to point out that the effective mass μ enters the ratio T/A only through the constant μ appearing in the derivatives v', u', and w'; this factors and cancels out of the ratio in Eq. (12), which makes the penetrability independent of the choice of effective mass.

D. Decay Half-Lives

The spontaneous-fission decay half-life from the ground-state level E_0 can be written as

$$T_0^{sf} = (\ln 2)(2\pi/\omega_0)[P(E_0)]^{-1},$$

where $P(E_0)$ is the barrier penetrability at E_0 and $2\pi/\omega_0$ is the time required for a single assault on the barrier. A reasonable estimate of the frequency ω_0 is 1 MeV/$\hbar$, which when substituted into the above equation yields

$$T_0^{sf} = 10^{-28.0}[P(E_0)]^{-1} \text{ yr}. \tag{13}$$

The spontaneous-fission half-life for the nucleus in question is determined by computing the zero-energy penetrability from Eq. (12) and substituting this value into Eq. (13).

The lifetime of the spontaneously fissioning isomer depends upon the penetrability through each of the two peaks surrounding the secondary minimum. These penetrabilities are computed from the WKB approximation

$$P(E) = \left\{1 + \exp\left[2\int_{\epsilon'}^{\epsilon''}\left(\frac{2\mu}{\hbar^2}[V(\epsilon) - E]\right)^{1/2} d\epsilon\right]\right\}^{-1}.$$

The integration limits ϵ' and ϵ'' are the values of ϵ on either side of the appropriate peak at which the integrand vanishes. The characteristic decay time in the fission direction – to the right from the intermediate well in Fig. 1 – is then determined from the equation

$$T^{sf}(E_i) = 10^{-28.0}[P^{sf}(E_i)]^{-1} \text{ yr},$$

where $P^{sf}(E_i)$ is the penetrability through the right-hand peak from the energy E_i of the isomeric state in the intermediate well. Furthermore, it has been shown in Ref. 29 that the half-life for γ decay from the isomeric state – decay back to the left from the intermediate well in Fig. 1 – can be estimated according to the equation

$$T^{g}(E_i) = 10^{-21.5}[P^{g}(E_i)]^{-1} \text{ yr},$$

where $P^{g}(E_i)$ represents the penetrability through the barrier to the left from the isomeric level E_i. The increased time for γ decay relative to spontaneous-fission decay reflects the required cou-

pling of two processes – penetration and γ decay – to return to the ground state. This asymmetry factor can help determine the left-right asymmetry of the barrier shape.

The total isomeric half-life is then given in terms of the partial half-lives by

$$T^i(E_i) = \left[\frac{1}{T^g(E_i)} + \frac{1}{T^{sf}(E_i)}\right]^{-1}$$

---

*Work performed under the auspices of the U. S. Atomic Energy Commission.

[1]W. D. Myers and W. J. Swiatecki, Nucl. Phys. 81, 1 (1966); Arkiv Fysik 36, 343 (1967).

[2]V. M. Strutinsky, Arkiv Fysik 36, 629 (1967); Nucl. Phys. A95, 420 (1967); A122, 1 (1968).

[3]S. M. Polikanov *et al.*, Zh. Eksperim. i Theor. Fiz. 42, 1464 (1962) [transl.: Soviet Phys. – JETP 15, 1016 (1962)].

[4]D. H. Byers *et al.*, U. S. Atomic Energy Commission Report No. CONF-660303, 1966 (unpublished), Book 2, p. 903.

[5]E. Migneco and J. P. Theobald, Nucl. Phys. A112, 603 (1968).

[6]D. Paya *et al.*, in *Proceedings of the Conference on Nuclear Data for Reactors, Paris, 1966* (International Atomic Energy Agency, Vienna, Austria, 1967), Vol. 2, p. 128.

[7]H. Weigmann, Z. Physik 214, 7 (1968).

[8]R. W. Lamphere and R. E. Greene, Phys. Rev. 100, 763 (1955).

[9]J. E. Lynn, Atomic Energy Research Establishment (Harwell) Report No. AERE-R 5891, 1968 (unpublished); J. E. Evans and G. A. Jones, private communication.

[10]J. A. Northrop, R. H. Stokes, and K. Boyer, Phys. Rev. 115, 1277 (1959).

[11]H. C. Britt, F. A. Rickey, Jr., and W. S. Hall, Phys. Rev. 175, 1525 (1968).

[12]N. Lark *et al.*, Nucl. Phys. A139, 481 (1969).

[13]R. Vandenbosch and K. L. Wolf, in *Proceedings of the Second Symposium on the Physics and Chemistry of Fission, Vienna, Austria, 1969* (International Atomic Energy Agency, Vienna, Austria, 1969), p. 439.

[14]S. C. Burnett *et al.*, Bull. Am. Phys. Soc. 14, 1210 (1969).

[15]V. Metag *et al.*, Z. Physik 226, 1 (1969).

[16]S. G. Nilsson *et al.*, Nucl. Phys. A115, 545 (1968); A131, 1 (1969).

[17]C. F. Tsang, University of California Lawrence Radiation Laboratory Report No. UCRL-18899, 1969 (unpublished).

[18]S. Bjørnholm and V. M. Strutinsky, Nucl. Phys. A136, 1 (1969).

[19]D. L. Hill and J. A. Wheeler, Phys. Rev. 89, 1102 (1953).

[20]B. B. Back *et al.*, in *Proceedings of the Second Symposium on the Physics and Chemistry of Fission, Vienna, Austria, 1969* (International Atomic Energy Agency, Vienna, Austria, 1969), p. 351.

[21]J. Pedersen and B. D. Kuzminov, Phys. Letters 29B, 176 (1969).

[22]A. V. Ignatyuk, N. S. Rabotnov, and G. N. Smirenkin, Phys. Letters 29B, 209 (1969).

[23]E. V. Gai *et al.*, in *Proceedings of the Second Symposium on the Physics and Chemistry of Fission, Vienna, Austria, 1969* (International Atomic Energy Agency, Vienna, Austria, 1969), p. 337.

[24]C. Y. Wong and J. Bang, Phys. Letters 29B, 143 (1969); in *Proceedings of the Second Symposium on the Physics and Chemistry of Fission, Vienna, Austria, 1969* (International Atomic Energy Agency, Vienna, Austria, 1969), p. 923.

[25]J. D. Cramer and J. R. Nix, in *Proceedings of the Second Symposium on the Physics and Chemistry of Fission, Vienna, Austria, 1969* (International Atomic Energy Agency, Vienna, Austria, 1969), p. 919.

[26]H. C. Britt, S. Burnett, and J. D. Cramer, in *Proceedings of the Second Symposium on the Physics and Chemistry of Fission, Vienna, Austria, 1969* (International Atomic Energy Agency, Vienna, Austria, 1969), p. 375; Bull. Am. Phys. Soc. 14, 1210 (1969).

[27]J. D. Cramer, Los Alamos Report No. LA-4198 (unpublished); European Office of the Air Research Development Command Report No. 131 "A," 1969 (unpublished).

[28]L. Moretto and W. J. Swiatecki, private communication.

[29]J. R. Nix and G. E. Walker, Nucl. Phys. A132, 60 (1969).

[30]N. Fröman and P. O. Fröman, *JWKB Approximation* (North-Holland Publishing Company, Amsterdam, The Netherlands, 1965).

[31]J. C. P. Miller, *Tables of Weber Parabolic Cylinder Functions* (Her Majesty's Stationery Office, London, England, 1955).